

EXPERIMENTAL STUDY OF EFFECT OF RECONDENSATION ON TYPE B CAI FORMATION IN THE PROTOSOLAR DISK. Y. Tsuruoka¹ and S. Tachibana¹, ¹Department of Earth and Planetary Science, The University of Tokyo, Hongo, Tokyo 113-0033, Japan; y-tsuruoka@g.ecc.u-tokyo.ac.jp.

Introduction: Calcium–aluminum–rich inclusions (CAIs), found in chondritic meteorites, are the oldest materials formed in the solar system. They consist of refractory minerals which are similar to the first phases to condense from a gas of solar composition [e.g., 1].

Type B CAIs are millimeter-to-centimeter-sized coarse-grained inclusions. They mainly consist of melilite, Al, Ti-rich calcic pyroxene (fassaite), anorthite, and spinel. They are textually subdivided into type B1s and type B2s [e.g., 1]. Type B1 CAIs have a continuous mantle of melilite ($\text{Ca}_2\text{Al}_2\text{SiO}_7$ (gehlenite)– $\text{Ca}_2\text{MgSi}_2\text{O}_7$ (åkermanite)) surrounding a core consisting of randomly distributed melilite, fassaite, anorthite, and spinel, while type B2 CAIs lack a melilite mantle. Petrological studies and experimental investigations have shown that type B CAIs have melted at $\sim 1400^\circ\text{C}$ above the melilite liquidus and crystallized from a liquid cooled at rates of $0.1\text{--}50^\circ\text{C hr}^{-1}$ [2–5].

The bulk compositions of type B CAIs are poor in Mg and Si compared to the composition of equilibrium condensate from a gas of solar composition, most likely due to kinetic evaporation of Mg and Si during melting.

Kamibayashi et al. (2021) [7] conducted crystallization experiments of type B CAI analog in low-pressure hydrogen gas [8]. They have shown that (1) effective evaporation of Mg and Si at $P_{\text{H}_2} \gg 1$ Pa results in their depletion at the rim, leading to crystallization of melilite from the surface (type B1-like structure) and (2) diffusion of Mg and Si in the melt dominates over their slower evaporation at $P_{\text{H}_2} \ll 1$ Pa, resulting in homogeneous crystallization of melilite in the melt (type B2-like structure). They concluded that the evaporation in $P_{\text{H}_2} > 1$ Pa is needed for the formation of type B1 CAIs.

Their experiments [7] were conducted in an open system, where no recondensation of evaporated species occurred [8]. However, evaporation of CAI melt could have occurred with recondensation of evaporated species [e.g., 9], which suppresses the evaporation and may affect the evaporation-induced crystallization of melilite.

Here we investigated the effect of recondensation during the crystallization of type B CAIs on their chemical and textural characteristics through laboratory experiments under protoplanetary disk-like conditions. The results are discussed to impose a new constraint on the hydrogen pressure of the protoplanetary disk during the type B CAI formation.

Methods: The experimental procedure is basically the same as [7]. The chemical composition of the starting material was similar to the composition χ on the trajectory of equilibrium condensation from a gas of solar composition at the total pressure of 1 Pa (hereafter referred to as $\text{CAI}\chi$) (25.71 wt% SiO_2 , 1.11 wt% TiO_2 , 33.23 wt% Al_2O_3 , 13.64 wt% MgO , and 26.30 wt% CaO) [10]. The same starting material was used in [7], in which preparation of $\text{CAI}\chi$ glass is described in detail.

A mixture of 20–40 mg of $\text{CAI}\chi$ glass was fixed onto a 2.5 mm-diameter iridium wire loop with polyvinyl alcohol [7, 8]. The samples were premelted in vacuum ($\ll 10^{-1}$ Pa) at 1600°C for 10 minutes and then at 1450°C for 10 hr using a vacuum furnace [7]. The premelted samples were spherical and 2–3 mm in size.

To conduct experiments in the presence of recondensation, some premelted samples were hung in one-side open platinum tubes. The hexagonal prism-shaped tubes were ~ 5 mm in length between two facing sides and 10 or 20 mm in height. More recondensation is expected to occur in a longer tube [11].

The evaporation-crystallization experiments under low-pressure hydrogen conditions were conducted at P_{H_2} of 1 Pa with a maximum temperature of 1420 or 1430°C in a vacuum furnace [7, 10, 12]. The maximum temperature was ~ 20 or 30°C higher than the liquidus temperature of melilite ($1402.5 \pm 2.5^\circ\text{C}$) of $\text{CAI}\chi$ [7].

The vacuum chamber was evacuated down to $< 5 \times 10^{-4}$ Pa. The samples were then preheated at $\sim 500^\circ\text{C}$ for ~ 1 hr to evacuate the adsorbed gas in the vacuum chamber. After the pressure becoming $< 5 \times 10^{-4}$ Pa at 500°C , the samples were heated to 1420 or 1430°C at a rate of $\sim 20^\circ\text{C min}^{-1}$. As soon as the temperature reached 1420 or 1430°C , hydrogen gas (99.99%) was introduced into the chamber. The hydrogen flow rate was controlled by a mass flow controller (Kofloc 3660) to retain the hydrogen pressure of 1 Pa. After heating for 1 hr at 1420 or 1430°C , the samples were cooled at a rate of 5 or 50°C hr^{-1} and quenched at 1100 or 1110°C by turning off the heater.

The sample weights were measured before and after the experiments using an electric ultra-microbalance (Mettler Toledo XP2U) to evaluate the evaporative weight loss of the melt. The samples were then mounted in epoxy and polished to expose the largest cross section. The internal textures and chemical compositions of minerals were observed and analyzed by a scanning electron microscope (JEOL JCM-7000) equipped with an energy dispersive X-ray spectrometer at U. Tokyo.

Results and Discussion: The samples after the experiments show igneous textures consisting mainly of melilite, spinel, pyroxene, and glass (Fig. 1). The absence of anorthite, which crystallize at 1260°C [3], does not affect the discussion of the crystallization of melilite in this study.

The texture of the samples differed depending on the cooling rates irrespective of the presence/absence of platinum tube; The sample cooled at a rate of 5°C hr⁻¹ showed a continuous mantle of melilite (Fig. 1(a)), while incomplete melilite mantles were observed in the samples cooled at a rate of 50°C hr⁻¹ (Fig. 1(b)), which is consistent with [7].

The chemical composition of melilite mantles in the sample heated in platinum tubes tends to have the higher åkermanite content than those in the samples heated in an open system (Fig. 2).

The weight loss of the samples cooled at a rate of 5°C hr⁻¹, normalized to the sample surface area, was 15.6, 7.8, and 7.5 mg cm⁻² for the sample heated in an open system, inside the 10 mm-height Pt tube, and inside the 20 mm-height Pt tube, respectively.

The smaller weight losses of the samples heated inside the platinum tubes indicate suppressed evaporation of Mg and Si due to recondensation [11]. Such suppressed evaporation of Mg and Si caused less effective enrichment of Ca and Al near the melt rim. This led to crystallization of melilite with a higher åkermanite content at the rim than those in the samples heated in the open system (Fig. 2).

In the present experiments, no textural difference was observed, but we confirmed that recondensation of evaporated Mg and Si affects the conditions under which the melilite mantles crystallize. Because the evaporation with recondensation is expected to occur in a dust-enrichment system [e.g., 13, 14], the hydrogen pressures required for the formation of type B1 and B2 CAIs would be a function of dust enrichment. Further constraints on dust enrichment during CAI formation would put a stronger constraint on the hydrogen pressure in the CAI forming region.

References: [1] MacPherson, G. J. (2014) In *Treatise on Geochemistry (Second Edition)* (H.D. Holland & K.K. Turekian, eds.), 139-179, Elsevier. [2] MacPherson, G. J. & Grossman, L. (1981) *EPSL* 52, 16-24. [3] Stolper, E. (1982) *GCA* 46, 2159-2180. [4] Stolper, E., & Paque, J. M. (1986) *GCA* 50, 1785-1806. [5] Yamamoto, D. et al. (2021) *GCA* 314, 108-120. [6] Grossman, L. et al. (2000) *GCA* 64, 2879-2894. [7] Kamibayashi, M. et al. (2021) *ApJ* 923, L12. [8] Mendybaev, R. A. et al. (2021) *GCA* 292, 557-576. [9] Richter, F. M. et al. (2007) *GCA* 71, 5544-5464. [10] Grossman, L. et al. (2002) *GCA* 66, 145-161. [11] Tachibana, S. et al. (2011) *ApJ* 736, 16. [12] Takigawa,

A. et al. (2009) *ApJ* 707, L97-L101. [13] Tsuchiyama, A. et al. (1999) *GCA* 63, 2451-2466. [14] Ozawa, K. & Nagahara, H. (2001) *GCA* 65, 2171-2199.

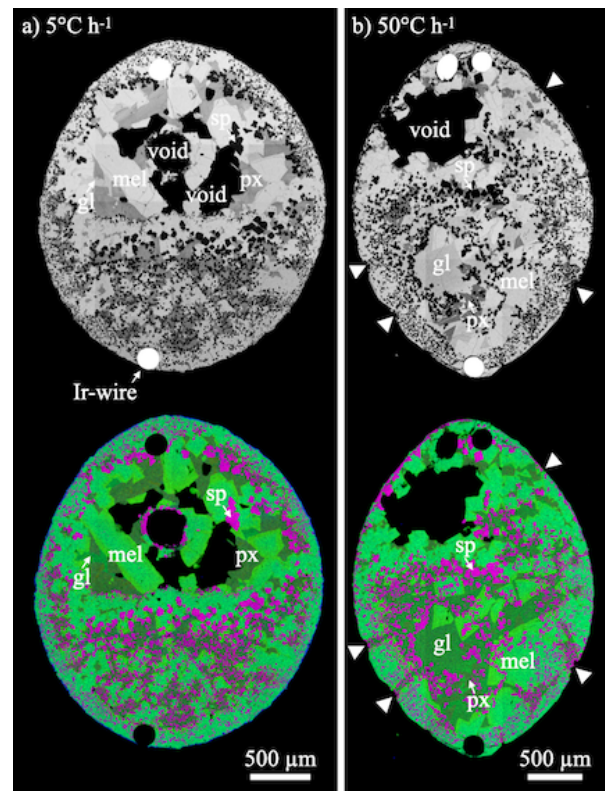


Fig. 1. Backscattered electron images and combined X-ray elemental maps with Mg (red), Ca (green), and Al (blue) in samples heated inside the 20 mm-height tubes. The samples were cooled at a rate of (a) 5°C hr⁻¹ and (b) 50°C hr⁻¹. Triangles indicate regions with no melilite mantle. gl = glass; sp = spinel; mel = melilite; px = pyroxene. Type B1- and B2-like structures were reproduced in (a) and (b), respectively.

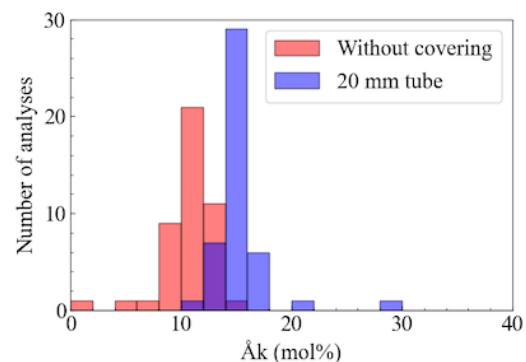


Fig. 2. Histograms of the compositions of melilite mantle measured at 50 μm distance from the sample surface. The samples were cooled at a rate of 5°C hr⁻¹ in an open system (red) or inside the 20 mm-height platinum tube (blue).